# Non-linear finite element analysis of grouted connections for offshore monopile wind turbines

Tziavos, Nikolaos; Hemida, Hassan; Metje, Nicole; Baniotopoulos, Charalampos

*DOI:*
10.1016/j.oceaneng.2018.11.005

# - -Manuscript OE_2018_455_R1- -

**Title:** Non-linear finite element analysis of grouted connections for offshore monopile wind turbines

**Authors:** Nikolaos I. Tziavos [a], Hassan Hemida [a], Nicole Metje [a], Charalampos Baniotopoulos [a]

**Corresponding Author:** Nikolaos I. Tziavos

**E-mail:** ntziavos@gmail.com

**Affiliations:** a) School of Engineering, Department of Civil Engineering, University of Birmingham, Edgbaston, Birmingham, B15 2TT, UK

**Word Count:** 5860 (Excluding abstract and references)

**Number of figures:** 18

**Number of tables:** 3

## - - Abstract - -

Grouted Connections (GCs) are vital structural components of Offshore Wind Turbine (OWT) substructures. On monopiles to achieve a GC, tubular hollow steel piles are in-situ attached with a high-strength grout. Monopiles are susceptible to large magnitude bending loads in offshore environments. Recently, following inspections the performance of GCs has been called into doubt when settlements were reported on several monopiles. To further comprehend the structural performance of GCs under large bending moments a nonlinear Finite Element (FE) analysis was conducted. Three-dimensional FE models were solved and validated against experimental and analytical data with good agreement. It is suggested that the presented models can be used to evaluate the global and local behaviour of a GC accurately. Finally, a comprehensive parametric study was carried out to investigate the influence of shear key numbers, shear key spacing and overlap lengths. It was shown that increased number of shear keys are advantageous for stiffness and reduce the gap at the interfaces, whereas the grout failure depends on the spacing between neighbouring shear keys. The ability of the numerical model to trace all relevant failure modes which are provoked by shear key spacing was also demonstrated.

**Keywords:** *Offshore Wind Turbines; Finite Element Analysis; Grouted Connections; Monopile; High-strength grout; Shear keys*

**Abbreviations**

| | |
|---|---|
| FE | **F**inite **E**lement |
| GC | **G**routed **C**onnection |
| O&G | **O**il and **G**as |
| OWT | **O**ffshore **W**ind **T**urbines |
| PGC | **P**lain **G**routed **C**onnection |

| | | |
|---|---|---|
| 34 | SKGC | **G**routed **C**onnection with **S**hear **K**eys |
| 35 | HSG | **H**igh **S**trength **G**rout |
| 36 | CDP | **C**oncrete **D**amage **P**lasticity |
| 37 | TP | **T**ransition **P**iece |
| 38 | | |

# 1. Introduction

Grouted Connections (GCs) are particularly favoured in offshore structures and their use has been common practice on Offshore Wind Turbines (OWTs) over the last decades. Their robustness has been proven within the Oil and Gas (O&G) sector, mainly when connecting piles with jacket legs or strengthening structural parts of offshore platforms [1]. On monopile OWTs, GCs are achieved by in-situ filling the annuli between overlapping tubular steel shells with a High-Strength cementitious Grout (HSG) (figure 1a). The grout attaches the monopile to the transition piece (TP), while allowing the transition from the substructure to the tower. It also ensures the vertical alignment of the latter, alleviating possible inclinations during installation. Owing to their arrangement, GCs are often referred to as pile to sleeve connections in the literature.

GCs on OWTs are based on the same principal with existing connections used in O&G structures. However, monopiles are characterised by large diameter-to-thickness ratios and the loading regime acting upon the substructure differs. Bending moments are the dominant effect on a monopile caused by the combined wind and waves action [2, 3]. In the early days of OWTs, inspections on monopiles revealed unexpected settlements of the TP on several turbines in Europe [1, 4]. The large magnitude bending loads on a GC result in high tensile stresses on the grout, which subsequently induces cracking in different directions. Furthermore, the ovalisation of the steel piles leads to a gap being formed at the steel grout interface [5]. As a result, the interface gaps lead to water ingress, which was also reported on some of the inspected monopiles [6].

Consequently, there has been increasing research interest on GCs aiming to enhance the design process. Particular attention is on monopiles due to the scale of the substructure and the scarce test data on large-diameter connections. Experimental campaigns have focused on data generation for GCs [see, e.g., 2, 3, 7] to comprehend the reasons that caused the unexpected slippages of the TPs on plain pipe connections.

Findings from these studies suggested the use of welded beads on the circumference of the tubular shells, known as shear keys, to provide mechanical interlock. Shear key types include semi-circular welded beads or fillet-welded square bars which are commonly fabricated within a central region of the connection as shown in figure 1b. As a result, design guidelines for GCs [8, 9] have been revised aiming to provide further assistance on the design of GCs with shear keys. Recently tests on GCs have focused on the fatigue performance of GCs [10]. To date, the use of tubular steel sections with circumferential shear keys or conical steel tubes without shear keys is the common approach for OWTs. However, as the connections are affected by numerous geometrical parameters (e.g., shear keys, grouted length, radial stiffness etc.) and environmental factors, further studies are needed to bridge the gap of knowledge on their structural performance.

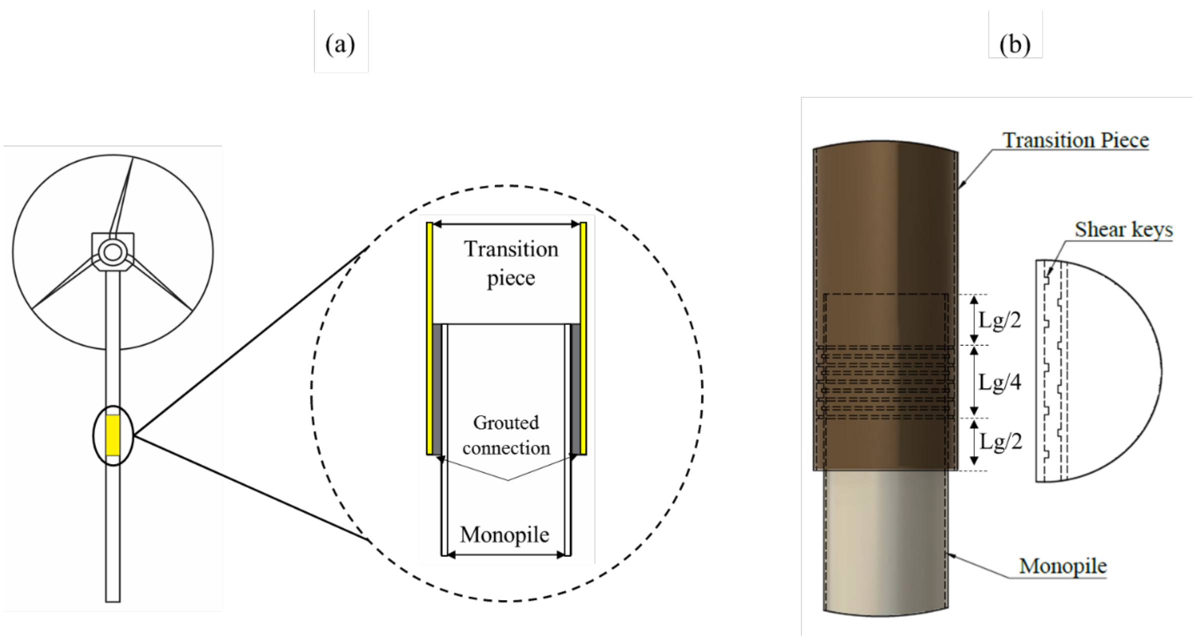


**Figure 1**: a) Layout of monopile with GC (after modification [4]) and b) GC with shear keys, where Lg refers to the grouted length

Apart from physical modelling, numerical methods are a promising alternative which compensate for the expenses of experimental campaigns. Finite Element (FE) analysis of GCs can be of remarkable benefit during the design process. It can provide a detailed insight on the grout condition as well as the load transfer mechanisms taking place in the connection. Additionally, parametric studies enable the investigation of numerous parameters once a validated model is achieved. Still, modelling of GCs is an intensive process when it comes to computational resources. This is due to the distinct brittle nature of the HSG, along with the interface modelling of steel, grout and shear key inclusion. Past studies [see, e.g., 7, 11, 12] tackled the intensity of the computations using numerical approaches of varying complexity.

A first attempt to provide general considerations for the numerical analysis of GCs is made by Nielsen [13]. A review of the available constitutive models for concrete-based material is presented along with a discussion on contact formulations. The degradation of the grout due to cyclic loading was not considered a major concern back then, as the consensus was that a HSG would compensate for those actions. The inclusion of shear keys was also not discussed as the practice was the installation of plain pipe connections. However, the sliding of TPs dictated the use of circumferentially-welded shear connectors and prompted researchers to include them in numerical analyses. Shear keys are usually a few millimetres in size which often leads to models with many elements requiring significant computational resources.  Fehling et al. [11] and Löhning and Muurholm [14] discussed alternative techniques to compensate for the additional computational effort induced from the inclusion of shear keys. Those involve the representation of shear keys with springs acting diagonally or vertically. A similar approach was employed by Wilke [7] for shear key representation. This method reduces the computational cost, however employing such an approach introduces a level of uncertainty as it requires the calibration of the spring stiffness with experimental data. Furthermore, it was shown that because of the de-bonding occurring at the interfaces it cannot be applied to regions where the shear keys lie close to the opening of the interface. In the case of monopiles gap opening between the steel and grout can be accounted as one of the reasons for insufficient performance and can develop significantly along the length of the connection.

Computational demand is also affected from the selected constitutive material models. Effective modelling of HSG requires the inclusion of cracking and crushing behaviour. Wang et al. [15] investigated the axial capacity of GCs using the brittle cracking model, whereas Andersen and Petersen [16] and [7] used the Drucker-Prager model to define the HSG. In the latter study is noted that the overall response of the connection was overestimated owing to the softening behaviour of the grout being supressed. [14] employed the Concrete Damage Plasticity (CDP) model to describe the grout behaviour of a plain pipe GC. The FE study focused on the interaction of bending and axial loads, however the model was only calibrated against an axially-loaded small scale GC without considering scale effects and differences in loading configuration.

Considering past studies [7, 11, 12] it was shown that the brittle nature of the grout, the interface modelling and the inclusion of shear keys, makes modelling of GCs a complex process. To date there is a lack of numerical studies with validated models focusing on the flexural behaviour of GCs with shear keys. This paper aims to present a consistent methodology to develop and validate three-dimensional numerical models of GCs, which can subsequently predict the failure modes that were found to be present on monopiles. Herein, in section 2, the experimental tests on down-scaled GCs which were used in this numerical study are briefly presented. Section 3 addresses the model specifics, such as mesh discretisation, material modelling and boundary conditions. Section 4, outlines the validation study conducted, while section 5 focuses on the parametric study to enhance the body of knowledge on the design of GC using FE analysis. Finally, in section 6 the conclusions of this work are presented.

## 2. Experimental tests on GCs for monopiles

In this study the experiments presented in [2, 7] are used to validate the numerical models. For this purpose, two GCs of approximately 1:6 scale were employed. The connections were loaded under a 4-point bending configuration. The tests were selected due to the documented failure modes being similar to those that were reported during the inspections of in-service monopiles. Experimental failure modes included grout cracking in the vicinity of shear keys, gap at the interface and deformation of the steel pile. The selected tests involve a plain pipe connection (PGC) and one with shear keys (SKGC). The dimensions of the GCs are given in Table 1, along with the DNV [9] recommended limits of application. Within Table 1 a non-dimensional parameter, the overlap length ($F_o$), is introduced. It is defined as the ratio of the grouted length over the pile diameter and is often used to compare GCs. It is worth noting that the examined GCs are of a lower overlap length than the limit suggested in [9].

## 3. FE modelling and numerical scheme

The following sections present the developed FE models and validation against the experimental data. For all the subsequent analyses the general-purpose FE software ABAQUS [17] was employed and a high-performance computational cluster was used for the computations. Three-dimensional models including geometrical and material non-linearity were solved by means of a quasi-static explicit analysis. The explicit method is a dynamic process, however when highly non-linear material behaviour and contact interactions are involved, it is an effective alternative to address convergence issues that often arise. This numerical approach has been effectively employed in previous studies, in a variety of structures involving concrete and interface problems [18, 19]. For the presented models, the computational cost was sufficiently reduced by using semi-automatic mass scaling with a fixed time increment of 4.5E-6 *s* in every step. A sensitivity analysis was performed to select the time increment, aiming to achieve a quasi-static solution by maintaining negligible inertia effects and artificial strain energy.

145

**Table 1.** Dimensions of FE models

| **Description** | **Symbol** | **Value**[1] | **Limit**[2] |
|---|---|---|---|
| Shear key height [mm] | $h$ | 3 | n/a |
| Shear key spacing [*mm*] | $s$ | 60 | n/a |
| Shear key width [*mm*] | $w$ | 6 | n/a |
| **Shear key ratio [-] | $h/s$ | 0.05 | < 0.1 |
| **Width to height ratio [-] | $w/h$ | 2 | $1.5 < \boldsymbol{w/h} < 3$ |
| Shear key number [-] | $n$ | 7 | |
| Pile, Sleeve length [*mm*] | $L_P$, $L_S$ | 1955 | n/a |
| Grout length [*mm*] | $L_g$ | 1040 | n/a |
| Pile diameter, thickness [*mm*] | $D_P$, $t_P$ | 800, 8 | $10 < \mathbf{R_P/t_P} < 30$ |
| Sleeve diameter, thickness [*mm*] | $D_S$, $t_S$ | 856, 8 | $9 < \mathbf{R_{TP}/t_{TP}} < 70$ |
| Grout diameter, thickness [*mm*] | $D_g$, $t_g$ | 840, 20 | n/a |
| Overlap length [-] | $F_o = L_g/D_P$ | 1.3 | $1.5 < \mathbf{L_g/D_P} < 3$ |
| End-beam length, thickness [*mm*] | $L_B$, $t_B$ | 1950, 14 | n/a |

[1]Wilke (2013),[2]DNV (2014), ** Applies only to the SKGC model

## 3.1 Model Geometry and Discretisation

A schematic representation of the FE models which are developed for the validation study is given in figure 2. The model geometry is developed to be identical to the experimental set-up. Throughout the models, 8-node solid elements with reduced integration (C3D8R) were used to discretise the grout and steel. Along the thickness of all parts a minimum of three elements were used. The end-beams were meshed with a larger element size compared to the pile, sleeve and grout to reduce the total number of elements. However, the size of the shear keys in the SKGC model led to an increased number of elements and a higher-density mesh on the grout was required. In order to appreciate the effect of shear keys on GC discretisation, on the PGC model approximately 37,000 elements were employed, whereas for the SKGC model a total of 93,042 elements. The shear keys were modelled as perfectly circular beads without considering welding irregularities to achieve higher mesh quality. For refinement purposes twelve elements were used along the circumference of each shear key as shown in figure 3, to achieve a perfectly-circular shear key geometry. Solution time is dictated from the element size in explicit computations, hence the SKGC model proved to be computationally-demanding when compared to the PGC as expected.

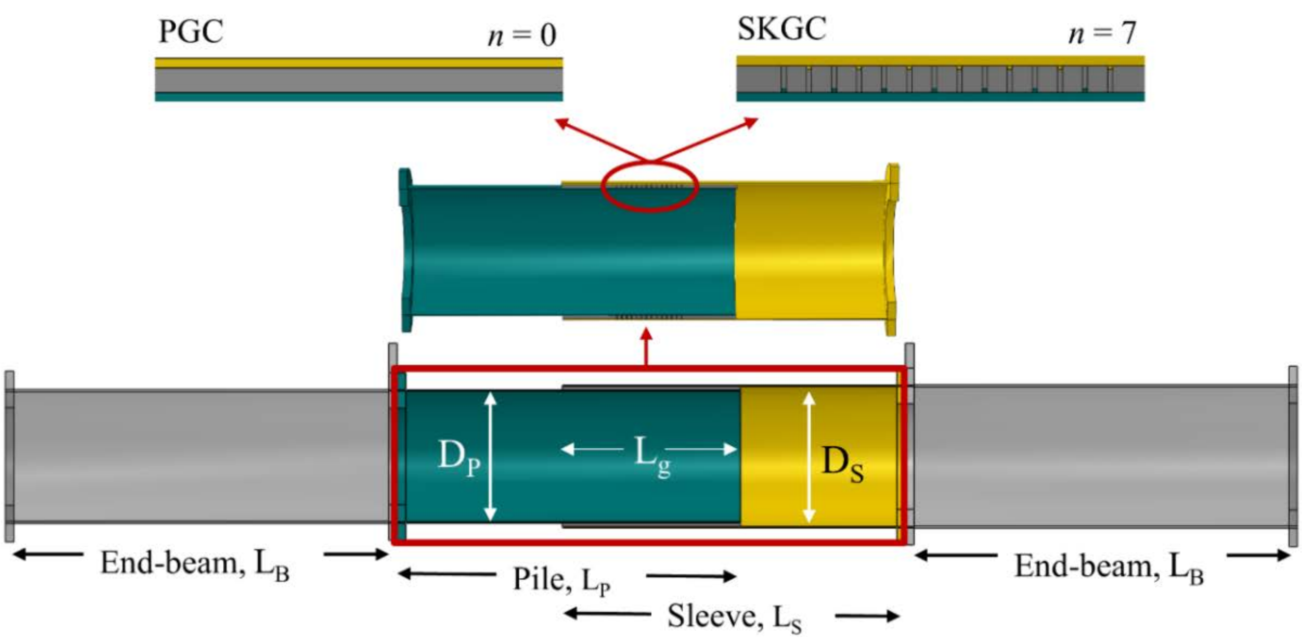


**Figure 2**. FE model definition of PGC and SKGC

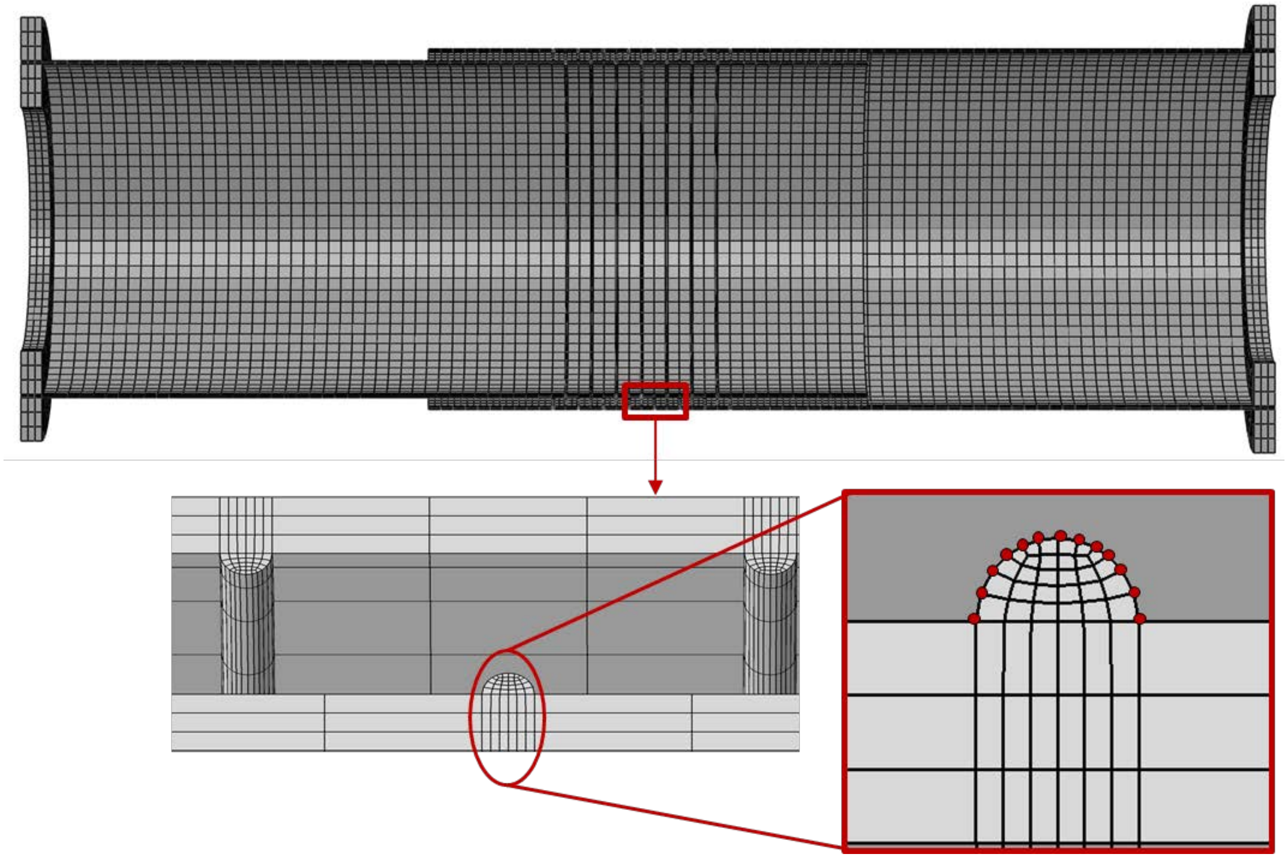

**Figure 3**. Meshed connection and discretisation around the cross section of a semi-circular shear key

## 3.2 Boundary conditions, constraints and interactions

Both PGC and SKGC were equipped with the same constraints and interaction properties for consistency. Parts of the test-rig and the spreader beam were not included in the numerical models and their role was simulated using appropriate constraints and boundary conditions reflecting the exact set-up presented in [7]. A detailed illustration of the selected constraints and applied boundary conditions used in the FE models is shown in figure 4.

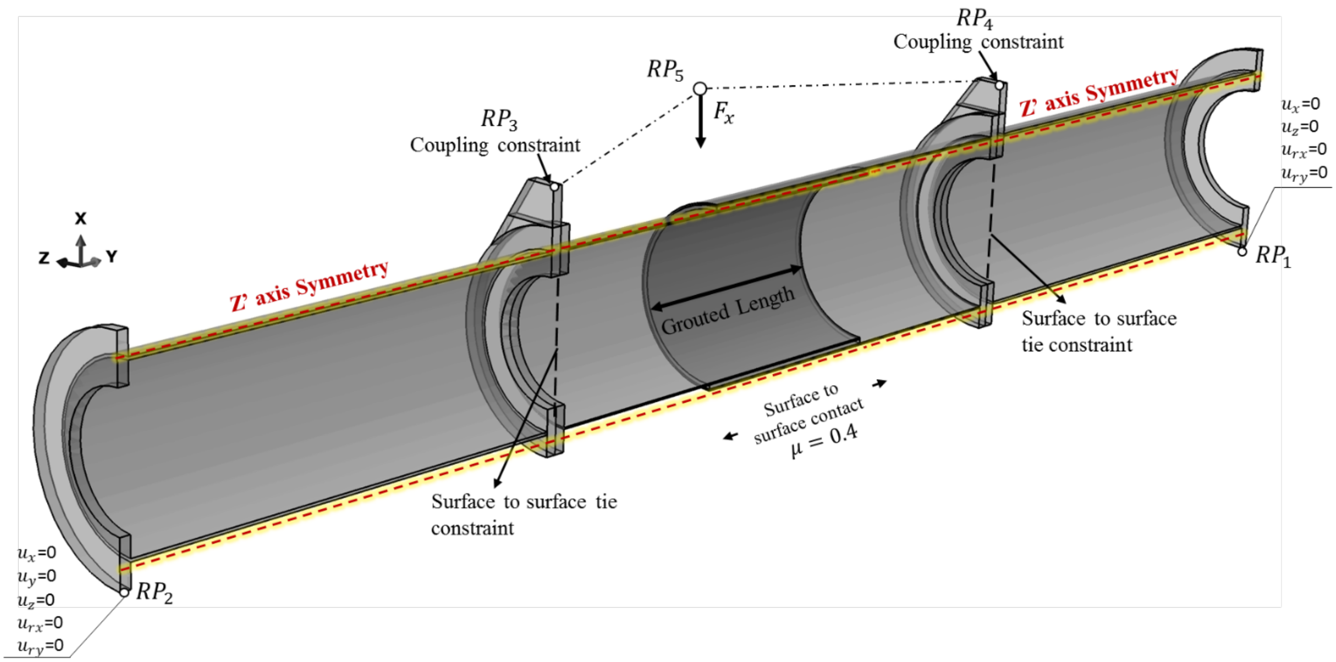


**Figure 4**. FE model description, boundary conditions and constraints

Initially, the symmetry of the assembly was exploited by modelling half of the specimen and applying a symmetry boundary condition towards $z$-axis. To apply the boundary conditions, reference points were introduced on the flanges. The node-sets of each flange are tied with kinematic coupling constraints to the corresponding reference points. The simply-supported boundary conditions were applied to reference points $RP_{1,2}$ as shown in figure 4. whereas the load was applied to reference points $RP_{3,4}$ with an eccentricity of 350 mm using a smooth amplitude function. The models were subjected to a load of 1000 *kN* and then unloaded to imitate the experimental campaign's loading scheme. Within this loading protocol, grout cracking, separation and yielding of the pile occurred. The end-beams were tied to the pile and sleeve with tie constraints to represent the bolted flanges that were used in test. The interactions between the grout, sleeve and pile were resolved with a surface to surface scheme. Hard contact was set in the normal direction, which allows for compressive stresses to be transferred at the interfaces and enables gap development between steel and grout. In the tangential direction a penalty contact formulation with a coefficient of friction of $\mu$ = 0.4 was selected.

## 3.3 Material modelling

### 3.3.1 Steel

The steel parts of the specimen were described as Elastic-Plastic with an isotropic hardening behaviour. The behaviour of the S235 steel tubes was defined according to the tensile coupon tests [7]. The true stress, $\sigma_{true}$, and strain, $\varepsilon_{true}$, curve was obtained from the engineering stress, $\sigma_{eng}$, and strain, $\varepsilon_{eng}$, following equations (1) and (2):

$$\sigma_{\text{true}} = \sigma_{\text{eng}}(1 + \varepsilon_{\text{eng}}) \tag{1}$$

$$\varepsilon_{\text{true}} = \ln\left(1 + \varepsilon_{\text{eng}}\right) - \left(\frac{\sigma_{\text{true}}}{\text{E}}\right) \tag{2}$$

The Young's modulus ($E$) and Poisson's ratio ($v$) was set to 210 *GPa* and 0.3, respectively. A density of 7850 $kg/m^3$ was used for steel.

### 3.3.2 High strength grout

A HSG was the employed cementitious medium with a mean compressive strength ($f_{cm}$) of 130 *MPa*. The material response of HSGs has similar characteristics to high and ultra-high strength concrete. In this direction, the CDP model [20, 21] is chosen in ABAQUS, which allows the definition of the grout behaviour in compression and tension and can trace crushing and cracking.

For the compressive behaviour of the material and to consider the confinement to some extent, the ascending branch was assumed to be linear until the peak strength is reached. In normal concrete, the peak strain ($\varepsilon_{c1}$) is often assumed to be equal to 0.0022, however this approach is limited to concrete with a compressive strength of up to 80 *MPa* [22]. Thereby, the peak strain was adjusted based on the analytical formulation proposed in [23] to better-reflect the HSG properties, which reads as:

$$\varepsilon_{c1} = \frac{0.7 {f_{cm}}^{0.31}}{1000} \tag{3}$$

Following the peak strain, the descending branch was set according to model-code CEB-FIP [22]. The damage variable $d_c$ ranged from 0 to 1 and was determined according to [18]:

$$d_c = 1 - (\frac{f_{cm}}{\sigma_c}) \tag{4}$$

where $\sigma_c$ is the stress corresponding to the inelastic strain.

To define the tensile behaviour of the grout the fracture energy approach [24] was adopted, as the strain formulation has been reported to cause numerical instabilities in concrete-related studies [25]. The fracture energy was determined from [22] as follows:

$$G_F = G_{F0} - \left(\frac{f_{cm}}{f_{cm0}}\right)^{0.7} \tag{5}$$

where $G_{F0}$ is the base value for fracture energy as a function of the aggregate size and $f_{cmo}$ = 10 *MPa*. Damage in tension was defined similarly to compression. The remaining properties of the HSG and the CDP parameters are summarised in Table 2. The global response of the model was found to be more sensitive to dilation angle ($\psi$) values, hence the selected value for the parameter must be based on the grout material used and should always be calibrated against experimental data. In this study, a value of $\psi$ = 38$^{o}$ was found to result in an appropriate global response when compared to test results.

**Table 2:** HSG properties and CDP parameters

| Description/Symbol | Value/Unit | CDP | Value |
|---|---|---|---|
| Modulus of Elasticity, $E$ | 50000 [$MPa$] | Dilation angle, $\psi$ | 38$^{o}$ |
| Poisson's ratio, $v$ | 0.19 | Eccentricity | 0.1 |
| Density, $\rho$ | 2380 [$kg/m^3$] | $\frac{\text{Compressive yield stress}}{\text{Uniaxial yield stress}}$ | 1.162 |
| Tensile strength, $f_t$ | 7 [$MPa$] | | |
| Fracture Energy, $G_F$ | 150.8 [$Nm/m^2$] | Viscosity | 0 |
| | | $K_c$ | 2/3 |

## 4. Model validation

The global behaviour of the FE models was validated by comparing load-deflection curves, stresses on the steel piles and interface opening. The notation which will be followed in the remaining sections is presented in figure 5a along with the locations where deflection and gap opening is measured unless otherwise stated. The pile and sleeve top correspond to 0 degrees, whereas the bottom to 180 degrees. The gap opening will always refer to the bottom of the GC at a location of 180 degrees. On both GCs pile yielding occurs at the bottom of the GC at 0 degrees (see figure 5b). Both models exhibited the expected interface de-bonding in the opposing top and bottom end, however in the SKGC model this was significantly reduced. The interface gap at the top and bottom of the connection was an expected outcome and was also documented in the test results.

The load-deflection curves for PGC and SKGC are plotted in figure 6a and 6b and the gap development from both models is depicted in figures 6c and 6d. Overall the FE models are in very good agreement with the experimental data and their ability to replicate the response of the specimens numerically is demonstrated. Finally, when comparing the peak displacement of the two models, a 6% higher deflection was observed for the PGC, which is almost identical to the one monitored during the tests.

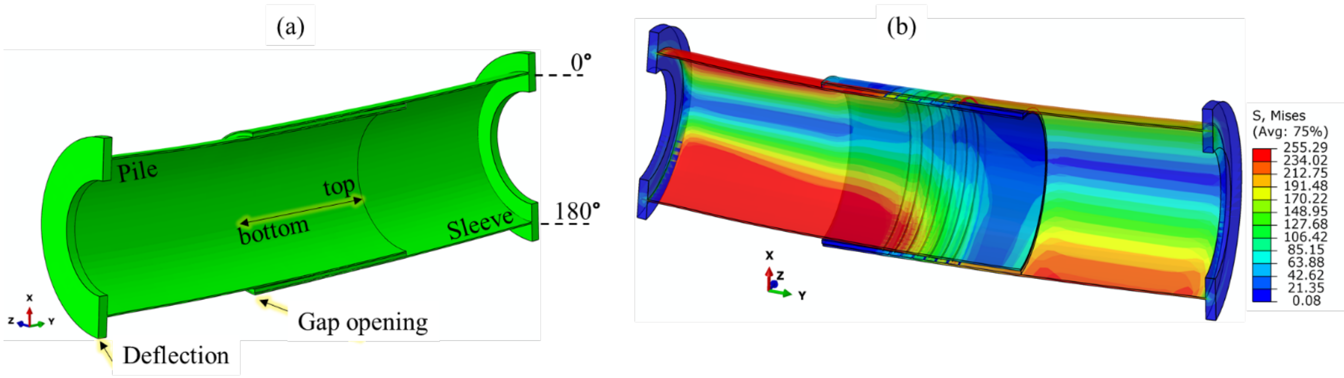


**Figure 5**. **a)** GC notation used for the FE models and **b)** Mises stresses on GC

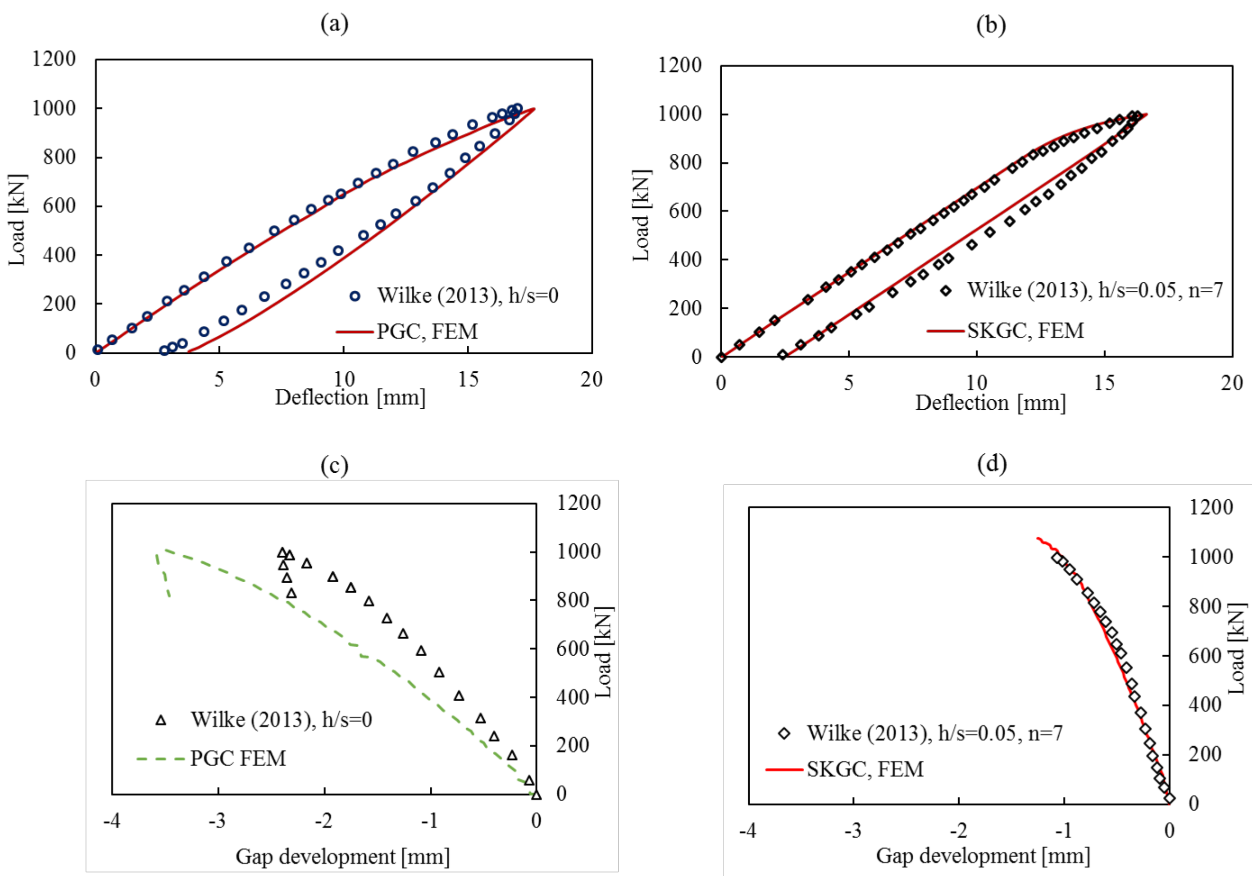


**Figure 6**. Load-deflection comparison between FE models and experimental data. a) PGC, b) SKGC. Load-gap opening curve for c) PGC and d) SKGC.

To enhance the validity of the FE models, the longitudinal stresses ($\sigma_{22}$) towards the length of the connection are also illustrated in figures 7 and 8. For both models, good agreement is achieved and only the stresses at the top of the PGC sleeve are slightly underestimated.

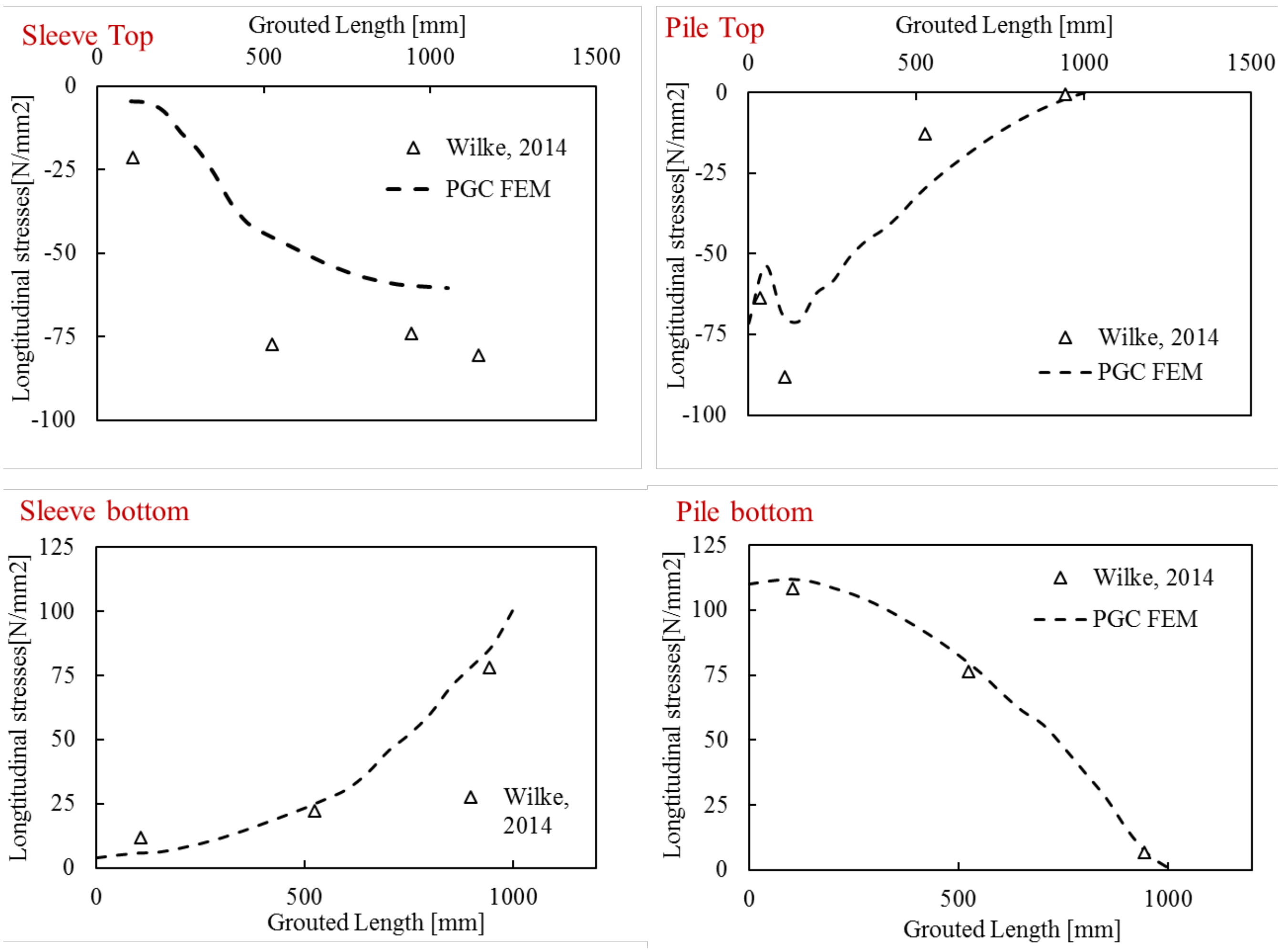


**Figure 7**. PGC longitudinal stresses at F = 435 kN

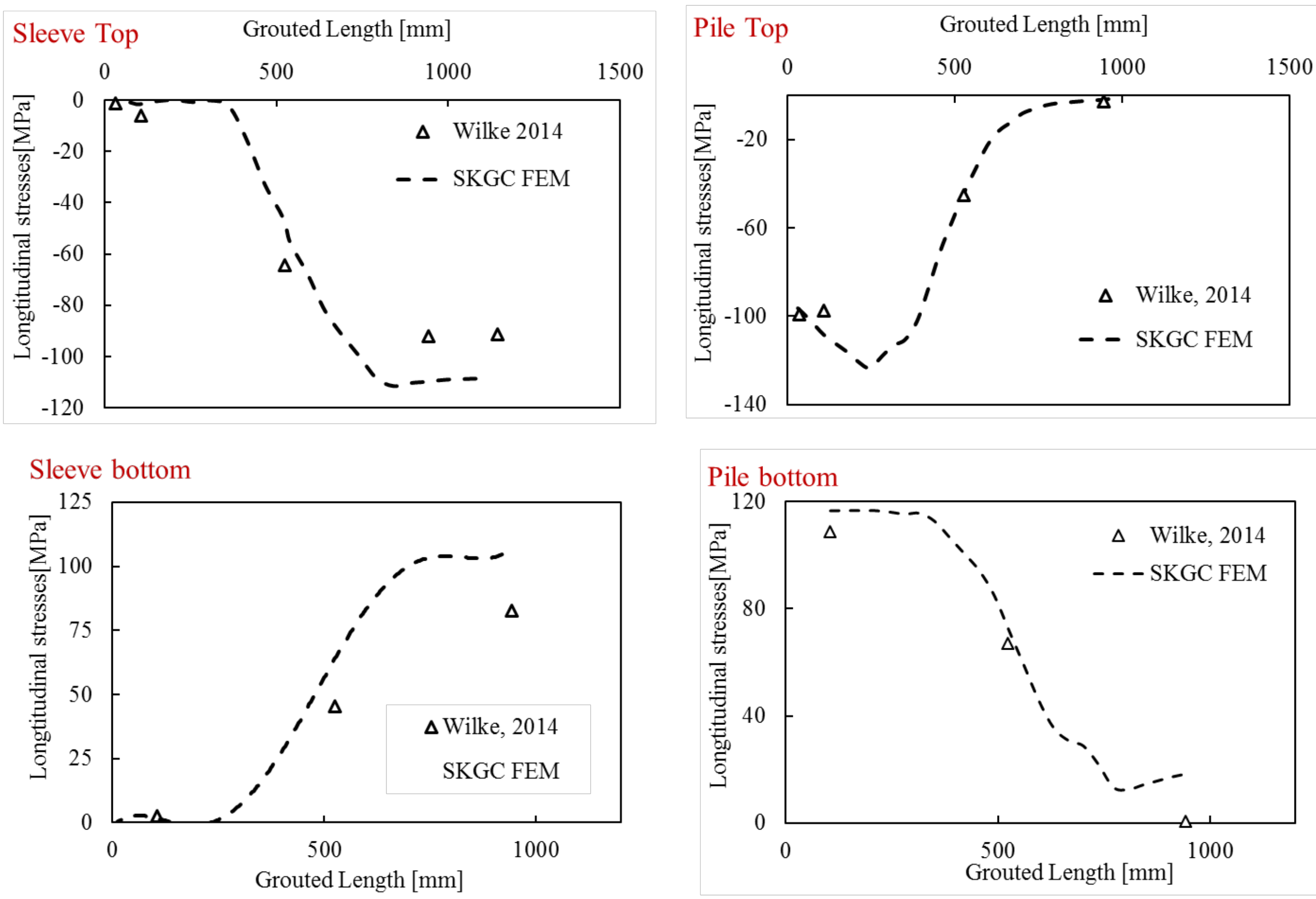


**Figure 8**. SKGC longitudinal stresses at F =435 kN

## 5. Parametric analysis

The verified FE models were taken forward to carry out a parametric study and provide further insight on the effect of geometrical parameters on the behaviour of GCs. The focus of the analyses was set on shear key parameters on GCs with various overlap lengths. More specifically, the number of shear keys ($n$) on each pile and the spacing ($s$) between them were examined. The main point of interest was initially the global behaviour of the model – involving stiffness and interface openings, and finally the local behaviour, focusing on crack patterns and failure modes. For illustration purposes two plain connections were also solved to highlight the interlock effect on the connection provided from the inclusion of shear keys.

A detailed description of the model geometries used in this study is given in Table 3. The tabulated dimensions refer to parts of the model that form the connection while the remaining steel tubes and ring-flanges were maintained as reported in Table 1. All investigated models were subjected to the same constraints, material properties and boundary conditions described in sections 2.1 and 2.2 to comply with the validation study and the same failure criterion was followed. The notation of the models is $\boldsymbol{F_{o,i} - n_i - s_i}$ ,where $F_{o,i}$ refers to overlap length and $n$, $s$ to the corresponding number of shear keys and spacing, respectively. For instance, $F_o15n7s50$ refers to a GC with $F_o = 1.5$ and 7 shear keys equally-spaced every 50 *mm*. For all the subsequent parametric models an effective number of shear keys ($n_{eff} = n+1$) has been used on the sleeve.

## 5.1 Shear key number

Experimental campaigns conducted to date, often involve connections with $F_o<1.5$, although this lies outside the recommended limits by DNV [9]. Initially, to demonstrate the benefit in bending stiffness with increasing grouted lengths, a typical force-displacement curve of selected models is shown in figure 9a. Models with shear keys are also included to demonstrate the superior performance exhibited when compared to plain connections. A series of numerical models with varying shear keys were developed to monitor their effect on the connection. In agreement with the validation study, the interface gap occurring at the opposing sides of the grout is minimised, with an increase in the number of shear keys (figure 9b), illustrating the considerable effect shear keys and grouted length have on the overall performance.

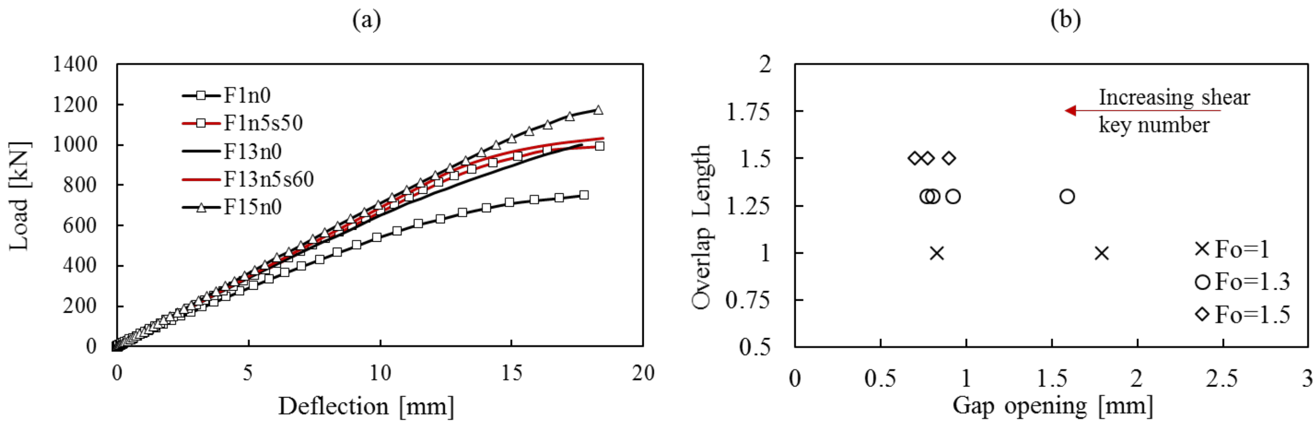


**Figure 9**. a) Force–displacement curve illustrating the effect of $F_o$, b) Maximum interface opening at GC bottom

In figure 10, a comparison of the global response of representative models dictates the benefits from increasing the number of installed shear keys. This is particularly pronounced for the lowest overlap length. From the parametric analysis it was observed that the influence of the shear key number is reduced for higher overlap lengths ($F_o$=1.5).

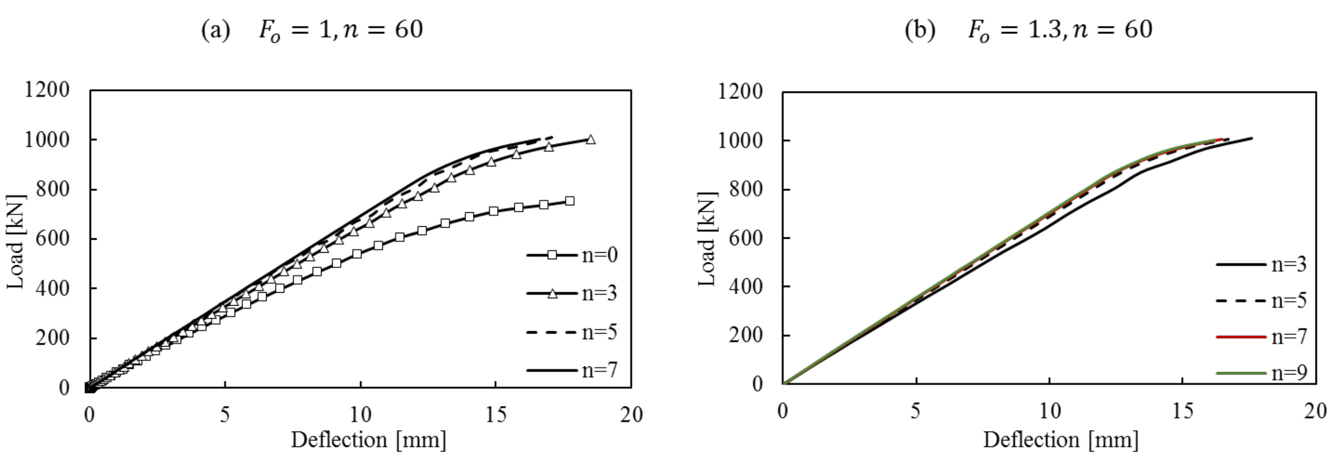


**Figure 10**. Force-deflection curves for: **a)** $F_o$=1, **b)** $F_o$=1.3

The gap that develops in the steel grout interfaces due to bending is of considerable interest, as it leads to water ingress. This is because it results in reduced friction between steel and grout, which can effectively disrupt the performance of the joint [26]. According to recent studies [27], GCs tested in dry environment have superior performance when compared to GCs in wet conditions.

To investigate the interface behaviour of the numerical models the maximum gap opening at the bottom of the connection was determined for the maximum applied load. Thereinafter, the results are compared with the analytical model proposed in [5] which is described in equations 6 to 8.

$$\mathrm{p}_{nom} = \frac{3\,\pi\, M_{tot}\, E\, L_g}{E L_g\left[R_p L_g^2(\pi+3\mu)+3\pi\mu R_p^2 L_g\right]+18\pi^2 k_{eff} R_p^3\left[\frac{R_p^2}{t_p}+\frac{R_{TP}^2}{t_{TP}}\right]} \tag{6}$$

where $\mathrm{p}_{nom}$ is the nominal contact pressure, $M_{tot}$ the total moment and $k_{eff}$ the effective spring stiffness which reads:

$$k_{eff} = \frac{2\, t_{TP} s_{eff}^2\, n\, E}{4\sqrt[4]{3(1-v^2)}\; t_g^2\left[\left(\frac{R_p}{t_p}\right)^{3/2}+\left(\frac{R_{TP}}{t_{TP}}\right)^{3/2}\right] t_{TP}+n s_{eff}^2 L_g} \tag{7}$$

where $s_{eff}$ is the effective spacing of shear keys reduced by one shear key width. Thus, the vertical opening can be calculated as follows:

$$\delta_u = \frac{6\mathrm{p}}{E}\frac{R_p}{L_g}\left(\frac{R_p^2}{t_p}+\frac{R_{Tp}^2}{t_{TP}}\right) \tag{8}$$

In figure 11, the opening that developed on GCs with $h/s$ = 0.05 is compared with the prediction from the analytical model. For most of the investigated geometries very good agreement was found. The biggest discrepancies between the numerical and analytical solutions appeared for the models with lower shear key numbers. It is apparent that an increased number of shear keys minimises the gap in the interface for all the examined grouted lengths.

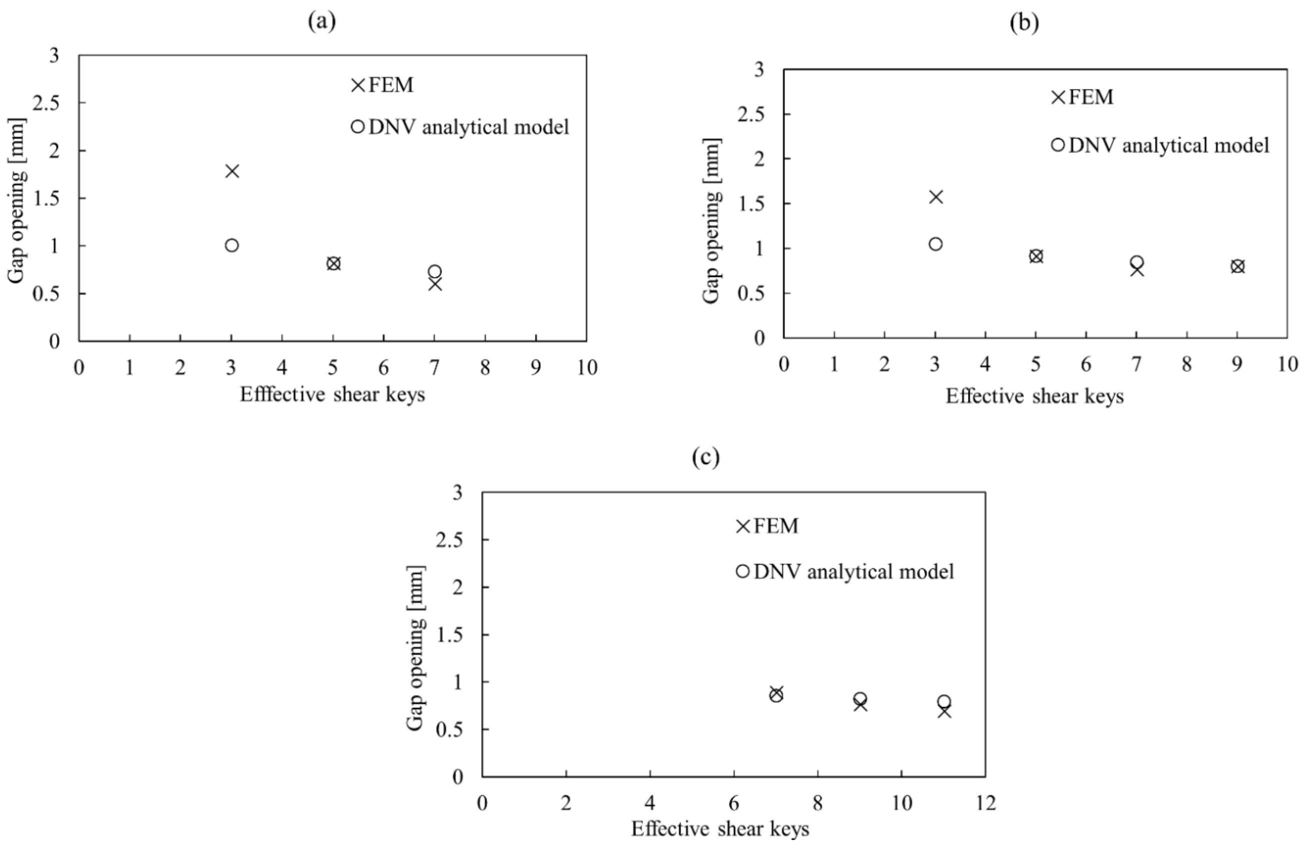


**Figure 11**. Maximum developed gap at $M_{max}$ for **a)** $F_o$=1, **b)** $F_o$=1.3, **c)** $F_o$=1.5

The use of shear keys alters the force transfer mechanism compared to a plain connection. The bending moments are mainly-transferred through the shear key region, which subsequently reduces the stresses at the top and bottom of the connection. This is illustrated in figures 12a and 12b where the pressure along the circumference of the sleeve is plotted for models with varying shear keys and overlap lengths. The stresses shown, are exerted on the inner sleeve surface, at the bottom of the GC following the notation of figure 5a. Three neighbouring circular paths on the sleeve were used to extract the stresses from the sleeve nodes. The data points shown in figure 12 depict the average values of the stresses from the three nodes on each location of the circumference. A fourth order polynomial is fitted to the data-sets to highlight the distribution of stresses along the circumference of the sleeve.

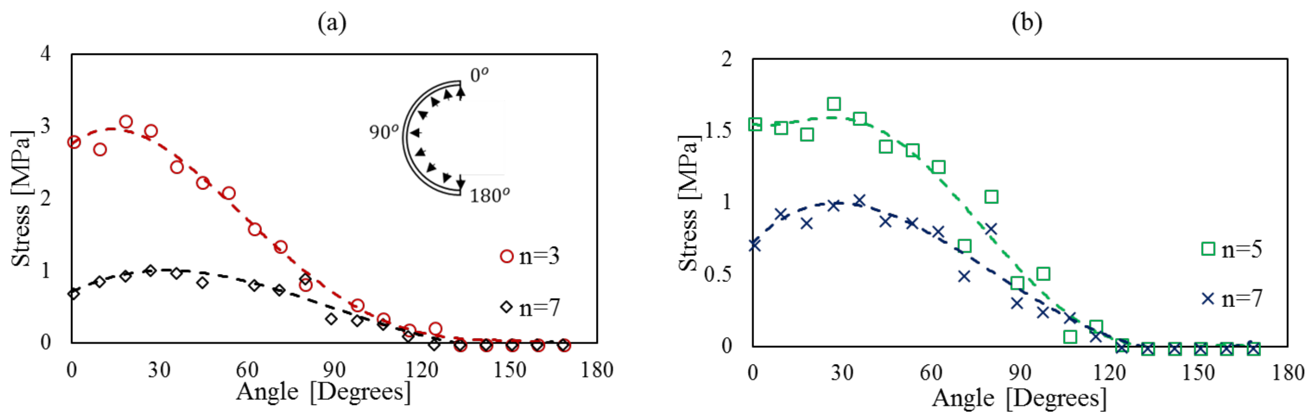


**Figure 12. a)** Contact pressure at maximum opening around the sleeve circumference for **a)** $F_o$=1, and **b)** $F_o$=1.3

Considering the results from the presented FE models an increase in the effective number of shear keys is shown to be beneficial as contact pressure reduces significantly at the measured location confirming that the stresses at the GC ends are reduced when using additional shear keys. Connections with a higher number of shear keys exhibit lower stresses, particularly in the region between $0^o$ and $90^o$ where contact pressure peaks. The stresses on the sleeve reduce to zero when approaching $180^o$ as opening has occurred at the tensile side of the tube. The findings are in agreement with previous studies [2, 7], as the shear-key region is now transferring a higher proportion of the applied loads when compared to a plain GC.

The alteration in load-transfer can also be realised if one considers the intensity of plastic strains in the shear key vicinity. In figure 13 the direction of plastic strains on a grout core are shown. The increased population of arrows in the tensile shear-keyed region depicts the damage occurrence taking place in this area.

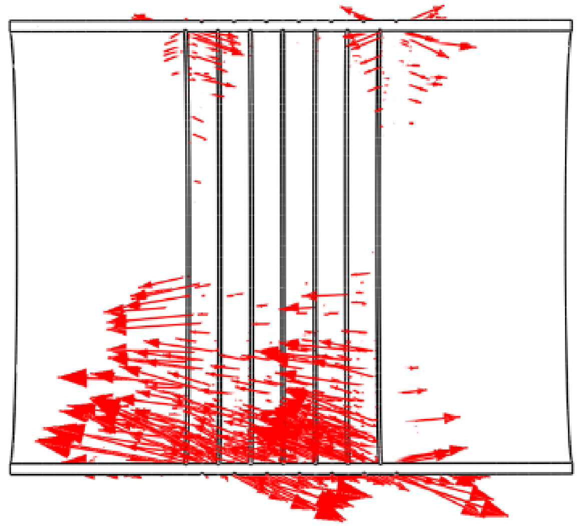

**Figure 13**. Grout plastic strain vectors at maximum load level

## 5.2 Grout failure modes

Previous experimental campaigns [7, 28] have noted that grout failure modes depend on shear key spacing. Due to spacing, cracking patterns within the grout core vary, from diagonal cracks with different inclinations between opposing shear keys, to cylindrical failure surfaces initiating at the tip of the shear keys. In all cases the grout failure in the shear key region typically develops along the circumference. Within this parametric study the ability of the FE model to capture the alternative failure modes of the grout based on shear key spacing has been examined. For this purpose, three representative FE models with varying shear key spacing ($s$ =30, 60, 120 mm) and a fixed overlap length ($F_o$= 1.3) were solved. The shear key height ($h$=3 mm) and the grout compressive strength (130 MPa) were kept constant for all GCs to isolate the effect of spacing. The selected distances resulted in the following ratios: $h/s$=0.025, 0.05, 0.1. In this study the CDP model was used, therefore cracking can be effectively traced by means of plastic strains.

In figure 14 iso-surface and banded contour plots of the grout plastic strains are illustrated. The location of interest is set on the tensile region of each GC focusing on the strut development based on the shear key positioning. For all the arrangements, cracking initiated at the tip of the shear keys as expected. For a spacing of 60 mm (figure 14a), cracks developed from pile and sleeve shear keys until they merge to form a diagonal strut which enables the load-transfer mechanism. Once the load increases additional wedged cracks form in front of the shear key. The inclination of the strut between two shear keys for this configuration was found to be 34$^{o}$ (figure 15a). This cracking behaviour compares well with findings reported on previous experimental studies involving GCs with similar shear key spacing and ratios [29]. Once the spacing of the shear keys was reduced to $s$=30 mm, the diagonal strut formed appeared with a steeper inclination of 53$^{o}$ as illustrated in figure 15b. Despite the high $h/s$ ratio the strut inclination was found to be within acceptable limits.

For $s$=120 mm the contour plots are shown in figures 14c, 15c. The increasing distance between the shear key leads to a very low shear connector ratio aiming to provoke the change in failure mode. Initially, due to the arrangement, the cracks initiated in front of the pile shear keys in contrast to the previous models. As loading increases cracks originate from the shear key tip until they reach the opposing pile or sleeve surface. Once failure of the strut has occurred, a cylindrically-shaped failure surface initiates circumferentially for all the shear keys. The same mechanism was reported for all shear keys of the GC. The angle of the diagonal cracking was calculated for all FE models based on ideal shear key distances and dimensions without considering welding irregularities.

With this section the robustness and ability of the numerical model to predict changing failure modes which are caused by shear key spacing was demonstrated convincingly. Thus, the presented numerical scheme can be used as a solid foundation for the design of GCs based on FEA.

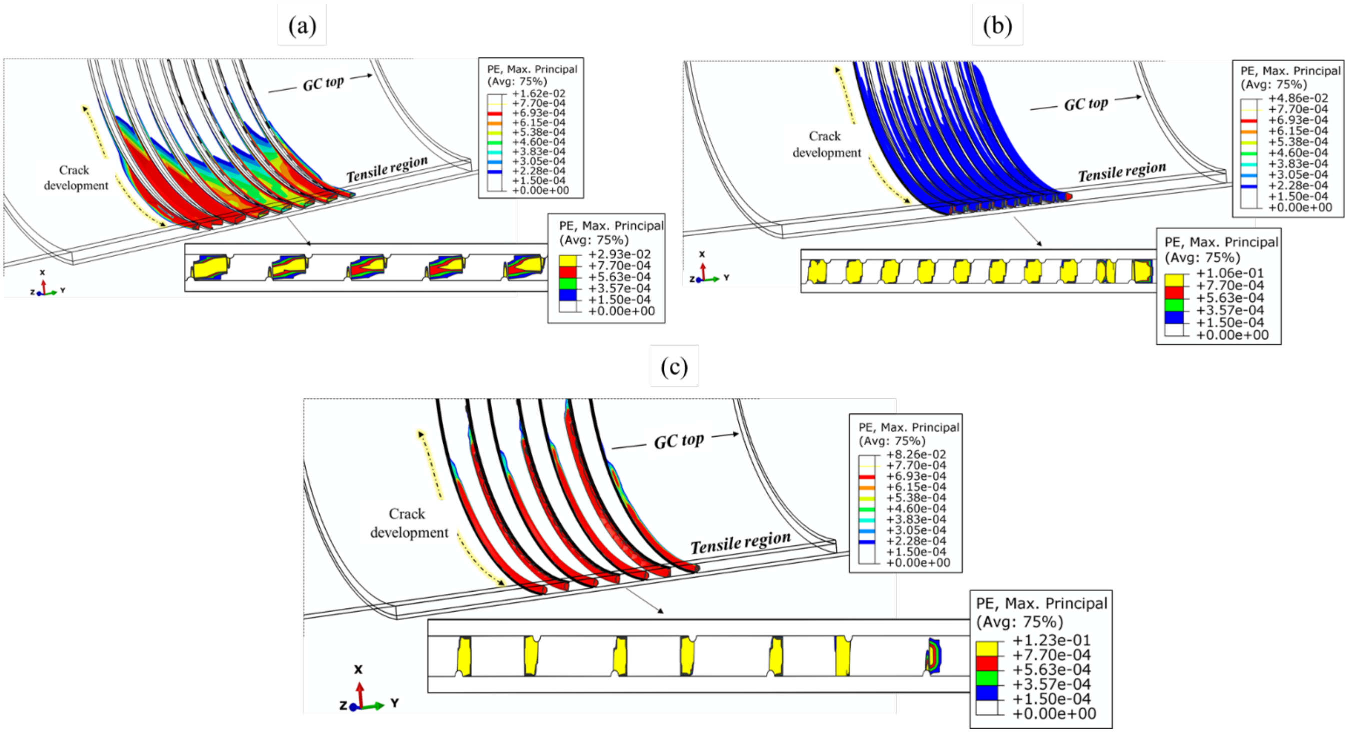


**Figure 14.** Iso-surface and contour plots of grout plastic strains for **a)** $s$=60 mm, **b)** $s$=30 mm, **c)** $s$=120 mm

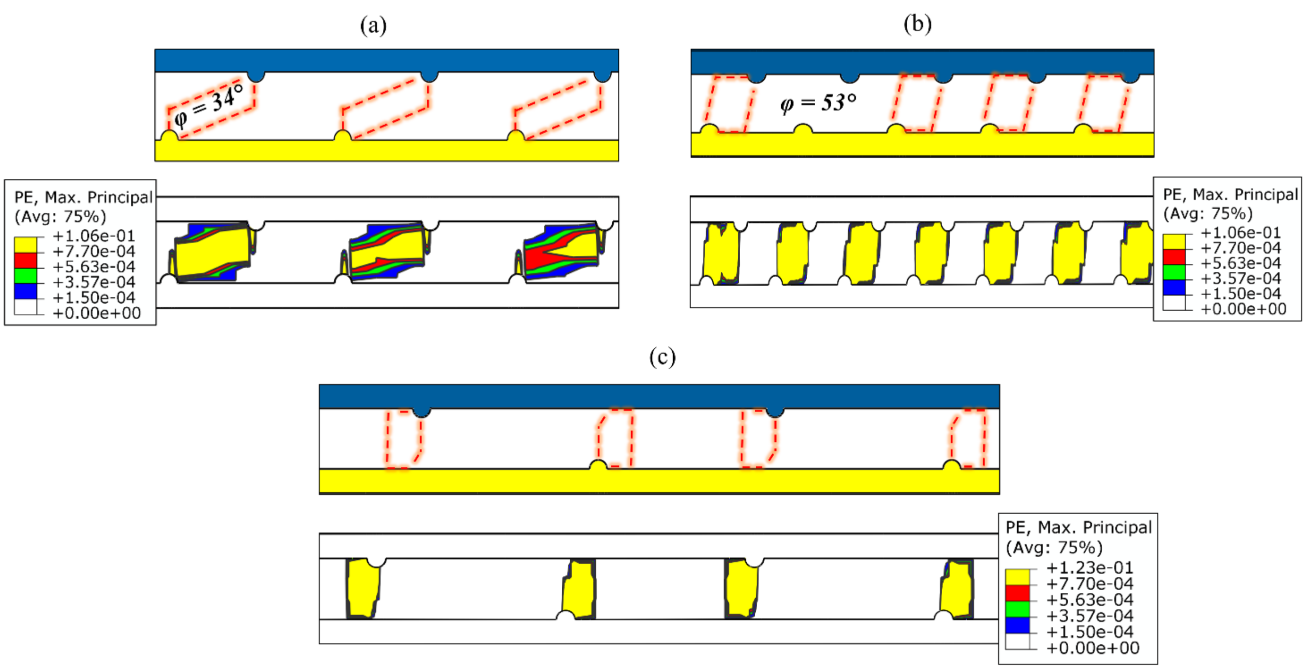


**Figure 15.** Grout failure modes for varying shear key spacing. **a)** $s$=60 mm, **b)** $s$=30 mm, **c)** $s$=120 mm

### 5.3 Shear key ratio

The upper limit suggested in design guidelines [9] for GCs with shear connectors is set to $h/s$<0.1, however, previous studies involving connections under bending have mostly employed lower shear key ratios from 0.02 to 0.05 [7, 28, 29]. Similar ratios can be found in the literature for axially loaded GCs. In order to study the influence of higher ratios, nine models with a ratio of 0.06 were numerically solved. To achieve this ratio the spacing between two consecutive shear keys was reduced to 50 *mm* maintaining the same height and width for the shear keys.

In figures 16a, b the maximum displacement is depicted for models of different overlap lengths. For comparison purposes, the location axis has been normalised against the total length between the pile and sleeve flange as shown figure 16. Therefore, a location equal to zero, corresponds to the displacement of the pile flange and a location equal to 1 corresponds to the sleeve flange. For all the analysed models with various $F_o$ a consistent pattern is noticed. Although a stiffer response is depicted for an increased overlap length and shear key number as discussed in section 4.2, increasing the shear key ratio did not improve the performance of the connection. The lower growth in displacement for GCs with $h/s$=0.05, resulted in a better bond action between the grout and steel. Likewise, with the results in section 4.1, for $h/s$=0.06 the influence of the parameter is noticeable for lower $F_o$, but significantly declines for $F_o$ = 1.5 (figure 16b).

In addition, as depicted in figure 17 the relative displacement which was found between the pile and sleeve for the parametric models is significantly higher for models with a shorter shear key region. Another deduction from figure 17 is that gaps on the interface can take place at lower load levels. Particularly for models with shorter shear key regions (see, e.g., $F_o1n3s50$ and $F_o15n3s60$) significant gaps occurred rapidly at $F$~$0.6F_{max}$.

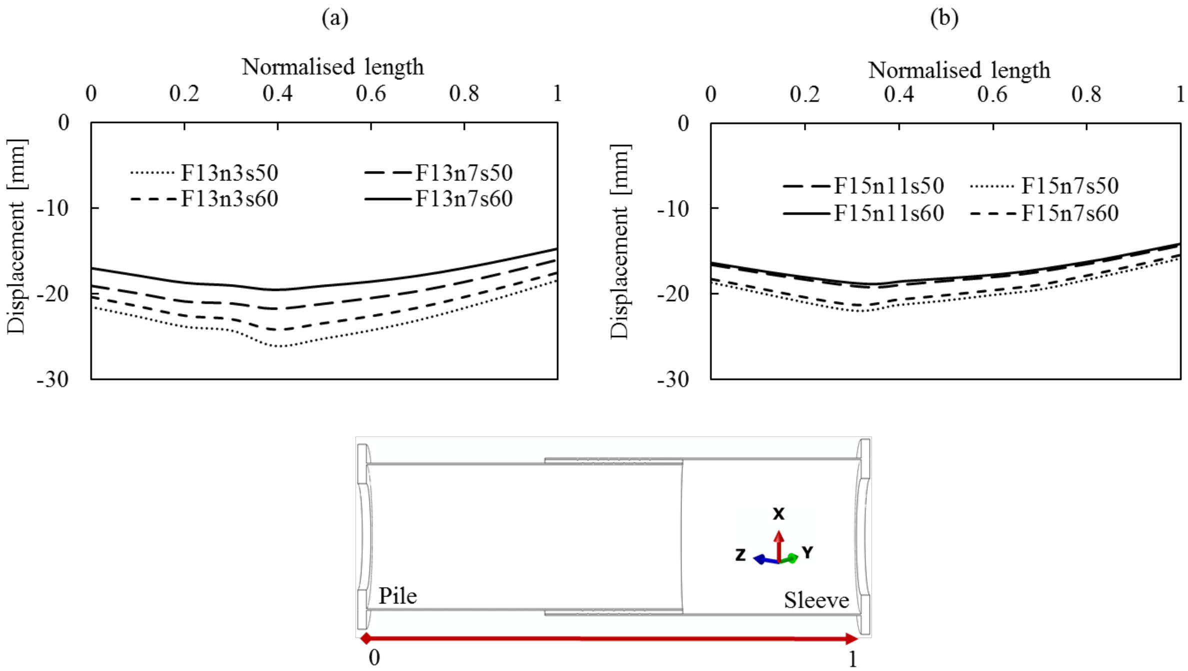


**Figure 16**. Displacement growth over normalised length for: **a**) $F_o$=1.3, **b**) $F_o$=1.5

(a)

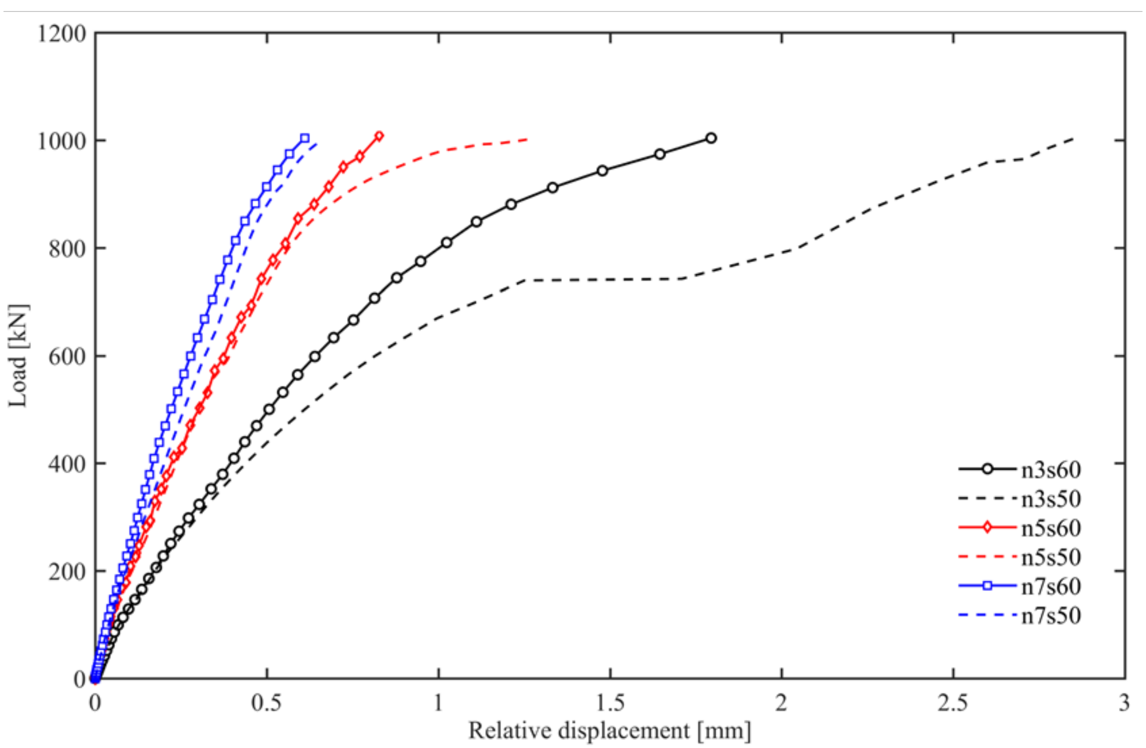

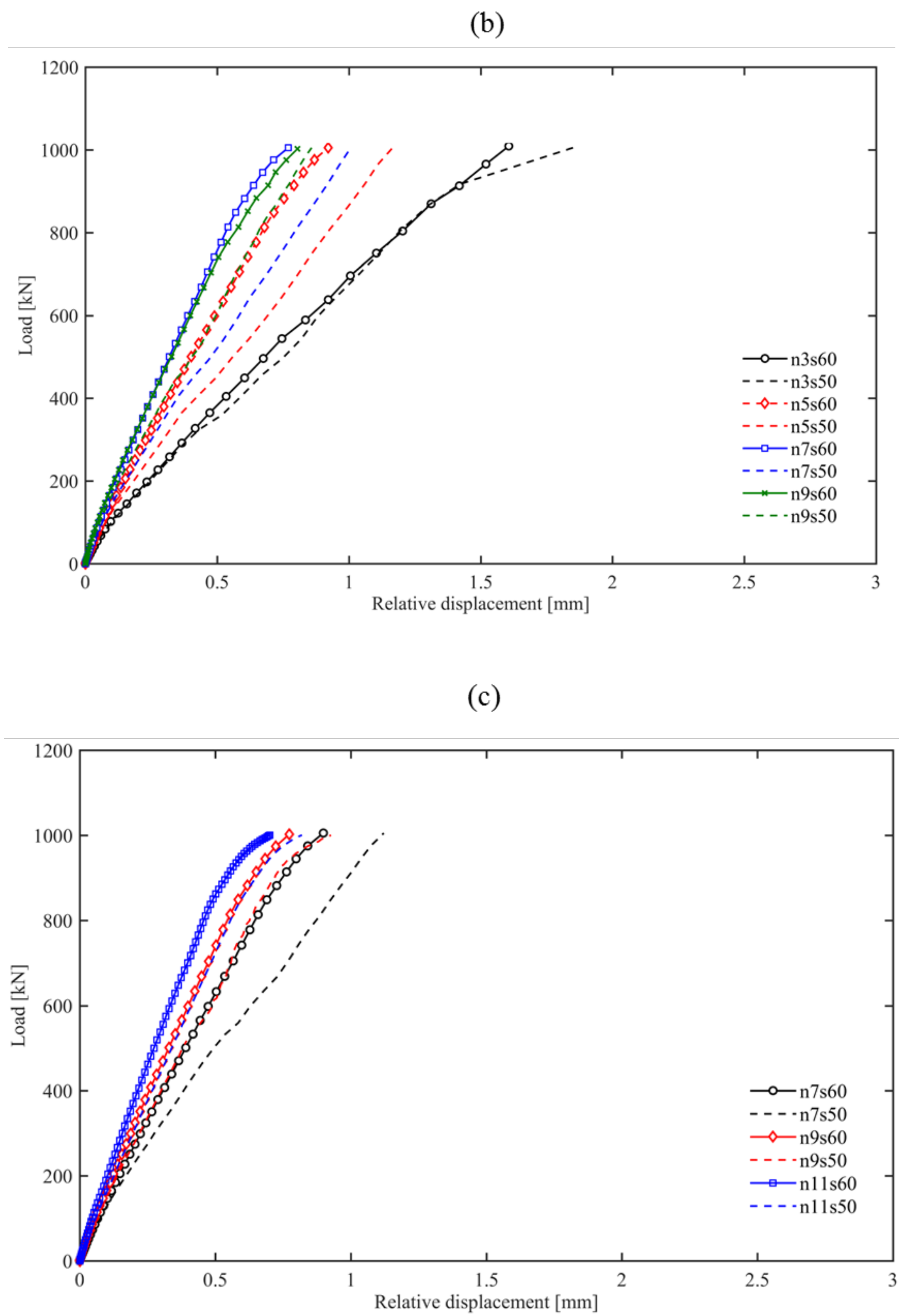


**Figure 17.** Force–Relative displacement for **a**) $F_o$=1, **b**) $F_o$=1.3, **c**) $F_o$=1.5

Finally, in figure 18 an overview of the interface gap calculated from the parametric models is presented as a function of the shear key region of each GC. The developed gaps form a plateau when the shear key regions are close to half the grouted length. However, it is evident that connections with shear keys in the middle third of the grouted length or less would benefit from a higher number of shear keys. An increasing number of shear keys is significantly reducing the de-bonding of the connection particularly for low overlap lengths.

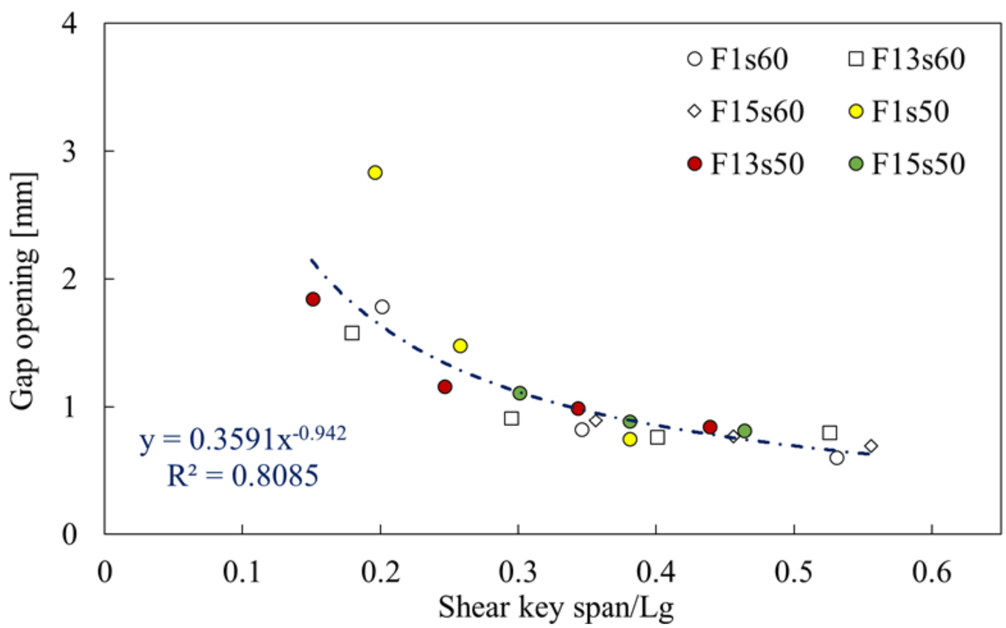


**Figure 18**. Maximum gap opening against shear key span from parametric models

**Table 3**. Geometrical characteristics of FE models for parametric analysis

| Name | $F_o$ | $n$ | Dimensions [mm] | | | | |
|---|---|---|---|---|---|---|---|
| | | | $L_{P,S}$ | $t_{s,p}$ | $h$ | $s$ | $L_g$ |
| $F_o$1$n$0$s$0 | 1 | - | 1835 | 8 | n/a | n/a | 800 |
| $F_o$1$n$3$s$60 | 1 | 3 | 1835 | 8 | 3 | 60 | 800 |
| $F_o$1n3$s$50 | 1 | 3 | 1835 | 8 | 3 | 50 | 800 |
| $F_o$1$n$5$s$60 | 1 | 5 | 1835 | 8 | 3 | 60 | 800 |
| $F_o$1$n$5$s$50 | 1 | 5 | 1835 | 8 | 3 | 50 | 800 |
| $F_o$1$n$7$s$60 | 1 | 7 | 1835 | 8 | 3 | 60 | 800 |
| $F_o$1$n$7$s$50 | 1 | 7 | 1835 | 8 | 3 | 50 | 800 |
| $F_o$13$n$0$s$0 | 1.3 | - | 1955 | 8 | n/a | n/a | 1040 |
| $F_o$13$n$3$s$60 | 1.3 | 3 | 1955 | 8 | 3 | 60 | 1040 |
| $F_o$13$n$3$s$50 | 1.3 | 3 | 1955 | 8 | 3 | 50 | 1040 |
| $F_o$13$n$3$s$120 | 1.3 | 3 | 1955 | 8 | 3 | 120 | 1040 |
| $F_o$13$n$9$s$30 | 1.3 | 9 | 1955 | 8 | 3 | 30 | 1040 |
| $F_o$13$n$5$s$60 | 1.3 | 5 | 1955 | 8 | 3 | 60 | 1040 |
| $F_o$13$n$5$s$50 | 1.3 | 5 | 1955 | 8 | 3 | 50 | 1040 |
| $F_o$13$n$7$s$60 | 1.3 | 7 | 1955 | 8 | 3 | 60 | 1040 |
| $F_o$13$n$7$s$50 | 1.3 | 7 | 1955 | 8 | 3 | 50 | 1040 |
| $F_o$13$n$9$s$60 | 1.3 | 9 | 1955 | 8 | 3 | 60 | 1040 |
| $F_o$13$n$9$s$50 | 1.3 | 9 | 1955 | 8 | 3 | 50 | 1040 |
| $F_o$15$n$0$s$0 | 1.5 | - | 2035 | 8 | n/a | n/a | 1200 |
| $F_o$15$n$7$s$60 | 1.5 | 7 | 2035 | 8 | 3 | 60 | 1200 |
| $F_o$15$n$7$s$50 | 1.5 | 7 | 2035 | 8 | 3 | 50 | 1200 |
| $F_o$15$n$9$s$60 | 1.5 | 9 | 2035 | 8 | 3 | 60 | 1200 |
| $F_o$15$n$9$s$50 | 1.5 | 9 | 2035 | 8 | 3 | 50 | 1200 |

| | | | | | | | |
|---|---|---|---|---|---|---|---|
| $F_o15n11s60$ | 1.5 | 11 | 2035 | 8 | 3 | 60 | 1200 |
| $F_o15n11s50$ | 1.5 | 11 | 2035 | 8 | 3 | 50 | 1200 |

# 6 Conclusions

Within this paper the behaviour of GCs for monopile OWTs has been investigated by means of detailed numerical computations aiming to enhance the existing knowledge by presenting robust FE models. The three-dimensional numerical models were solved employing a quasi-static approach with an explicit analysis, which was effectively used reducing the computational cost and accomplishing results of high accuracy. The HSG was modelled with the CDP model and the non-linear aspects of the material were included in the numerical models. The key parameters of the material behaviour were discussed in detail and attention was drawn to the dilation angle value, which in lack of supporting material data, is recommended to be calibrated using a sensitivity analysis.

The FE models were able to detect cracking of the grout core accurately along with the corresponding failure modes. Primary diagonal cracking between neighbouring shear keys was the failure mode of FE models with $h/s$ = 0.05, 0.06 whereas cylindrical failure surfaces were monitored for GCs with increased spacing between shear keys. A high level of refinement of the meshed parts is highly recommended for the shear key region in order to capture the cracks occurring in the grouted region. The notion that the grout can accommodate the load-transfer process on the connection even after cracking was also confirmed, however cracking initiation occurred at low load levels when the connection is subjected to bending.

The complex interacting interfaces were modelled with a Coulomb-friction model. A friction coefficient $\mu$ = 0.4 yielded excellent agreement against the selected experimental data set. All models developed interface gaps at opposing sides of the connection and the results were in excellent agreement with an analytical model [5]. Reflecting on the above, it can be concluded that the steel-grout bond and the damage on the grout can be modelled combining the CDP model, a Coulomb-friction model and a fine mesh in the areas of interest.

From the parametric study, the plain GCs which were mainly used for comparison purposes exhibited the anticipated lower performance and a pronounced de-bonding of the interface. On the other hand, the mechanical interlock provided by the shear keys led to a superior behaviour of the GCs with shear keys. The use of shear keys imposed a smoother stress distribution at the connection ends, while cracking occurred in the shear key region due to the fact that the majority of the load was transferred from the middle part of the connection. Interface opening was also found to be limited when increasing the number of shear keys.

Contrary to the impact of increasing shear key numbers, the higher shear key ratio did not yield superior performance owing to the change of grout failure. The relative displacement between the pile and sleeve calculated in all the numerical models revealed that shear key regions on the steel tubes occupied by shear keys is of equal importance to the height and spacing. Finally, based on the presented FE models, overlap lengths equal to unity should be avoided as the stress intensities are increased. It was also shown that the grouted length of the connection is of significant importance to the performance of the connection.

## Acknowledgments

The authors would like to acknowledge the Birmingham Environment for Academic Research (BlueBEAR) for providing the computational resources for this work. This research project is funded by the School of Engineering at the University of Birmingham, UK, and the financial support the first author received, is gratefully acknowledged. The first author would also like to acknowledge the *WINERCOST COST Action TU1304* for funding a Short Term Scientific Mission (STSM) at Leibniz

University Hannover. The last author acknowledges with thanks the Alexander von Humboldt – partial shifting for the support of his research authority.

# REFERENCES


[1] Dallyn, P., El-Hamalawi, A., Palmeri, A. and Knight, R. (2015). Experimental testing of grouted connections for offshore substructures: a critical review. Structures, 3: pp. 90–108. https://doi.org/10.1016/j.istruc.2015.03.005

[2] Schaumann, P., Lochte-Holtgreven, S. and Wilke, F. (2010). Bending tests on grouted joints for monopile support structures. In *Proceedings of the 10th German Wind Energy Conference* (DEWEK), Bremen, Germany.

[3] Lotsberg, I., Serednicki, A., Oerlemans, R., Bertnes, H. and Lervik, A. (2013). Capacity of cylindrical shaped grouted connections with shear keys in offshore structures. The Structural Engineer, 91(1), pp.42-48.

[4] Tziavos, N.I., Hemida, H., Metje N. and Baniotopoulos, C. (2016). Grouted connections on offshore wind turbines: A review. Engineering and Computational Mechanics (ICE), Themed issue on offshore wind, 169(4), pp. 183-195. https://doi.org/10.1680/jencm.16.00004

[5] Lotsberg, I. (2013). Structural mechanics for design of grouted connections in monopile wind turbine structures. Marine Structures, 32, pp. 113–135. https://doi.org/10.1016/j.marstruc.2013.03.001

[6] Brett, C.R., Gunn, A.D., Dashwood, B.A.J., Holyoake, S.J. and Wilkinson, P.J. (2018). Development of a technique for inspecting the foundations of offshore wind turbines. Insight – Non-Destructive Testing and Condition Monitoring, 60(1).

[7] Wilke, F. (2013). *Load Bearing Behaviour of Grouted Joints Subjected to Predominant Bending*. Doctoral Dissertation, Institute for Steel Construction, Leibniz Universität Hannover, Hannover, Germany.

[8] DNV (2011) DNV-OS-J101. Offshore Standard: Design of offshore wind turbine structures. Det Norske Veritas AS.

[9] DNV (2014) DNV-OS-J101. Offshore Standard: Design of offshore wind turbine structures. Det Norske Veritas AS.

[10] Chen, T., Wang, X., Yuan, G. K., and Liu, J.C. (2018) Fatigue bending test on grouted connections for monopile offshore wind turbines. Marine Structures, 60, pp. 52-71.

[11] Fehling, E., Leutbecher, T., Schmidt, M. and Ismail, M. (2013). Grouted connections for offshore wind turbine structures. Steel Construction, 6(3), pp.216-228. https://doi.org/10.1002/stco.201310031

[12] Löhning, T., Voßbeck, M. and Kelm, M. (2013). Analysis of grouted connections for offshore wind turbines. Proceedings of the Institution of Civil Engineers-Energy, 166(4), pp.153-161. https://doi.org/10.1680/ener.12.00009

[13] Nielsen, L.P. (2007). Finite element analysis of large diameter grouted connections. In Proceedings of the 26th International Conference on Offshore Mechanics and Arctic Engineering. San Diego, CA, USA, pp.449-457. https://doi:10.1115/OMAE2007-29199

[14] Löhning, T. and Muurholm, U. (2013). Design of grouted connections in offshore wind turbines. In IABSE Symposium Report, 99(13), pp. 1252-1259.

[15] Wang, Z., Zhang, Y., Chen, F., Wang, G., Wang, L., Jiang, J. (2017). Axial bearing capacity of large-diameter grouted connections analysed by means of a simplified double shear test. Construction and Building Materials, 134, pp. 245-253.

[16] Andersen, M.S. and Petersen, P. (2004). Structural design of grouted connection in offshore steel monopile foundations. In *Proceedings of Global Windpower Conference*, Chicago, USA.

[17] Abaqus (2013). ABAQUS 6.13 Documentation Collection, Dassault Systèmes Simulia Corp., Providence, RI, USA.

[18] Pavlović, M., Marković, Z., Veljković, M. and Buđevac, D. (2013). Bolted shear connectors vs. headed studs behaviour in push-out tests. Journal of Constructional Steel Research, 88, pp.134-149. https://doi.org/10.1016/j.jcsr.2013.05.003

[19] Liu, X., Bradford, M.A., Chen, Q.J. and Ban, H. (2016). Finite element modelling of steel–concrete composite beams with high-strength friction-grip bolt shear connectors. Finite Elements in Analysis and Design, 108, pp.54-65. https://doi.org/10.1016/j.finel.2015.09.004

[20] Lubliner, J., Oliver, J., Oller, S. and Onate, E. (1989). A plastic-damage model for concrete. International Journal of solids and structures, 25(3), pp.299-326. https://doi.org/10.1016/0020-7683(89)90050-4

[21] Lee, J. and Fenves, G.L. (1998). Plastic-damage model for cyclic loading of concrete structures. Journal of Engineering Mechanics, 124(8), pp.892-900.

[22] CEB-FIP, M (1990). Model code for concrete structures. Bulletin D' Information.

[23] Tomaszewicz, A. (1984). Betongens Arbeidsdiagram. SINTEF report N$^{0}$ STF 65A84065, Trondheim, Norway. *In*: Van Gysel, A. and Taerwe, L. (1996). Analytical formulation of the complete stress-strain curve for high strength concrete. Materials and Structures, 29, pp. 529-533.

[24] Hillerborg, A., Modéer, M. and Petersson, P.E. (1976). Analysis of crack formation and crack growth in concrete by means of fracture mechanics and finite elements. Cement and concrete research, 6(6), pp.773-781.

[25] Abdelatif, A.O., Owen, J.S. and Hussein, M.F. (2015). Modelling the prestress transfer in pre-tensioned concrete elements. Finite Elements in Analysis and Design, 94, pp. 47-63. https://doi.org/10.1016/j.finel.2014.09.007

[26] Schaumann, P., Raba, A. and Bechtel, A. (2016). Impact of Water on the Fatigue Performance of Large-Scale Grouted Connection Tests. In ASME 2016 35th International Conference on Ocean, Offshore and Arctic Engineering. Busan, South Korea, 19-24 June. https://doi:10.1115/OMAE2016-54823

[27] Schaumann, P., Raba, A. and Bechtel, A. (2017). Fatigue behaviour of grouted connections at different ambient conditions and loading scenarios. Energy Procedia, 137, pp. 196-203.

[28] Lamport, W.B. (1988). *Ultimate strength of grouted pile-to-sleeve connections.* Doctoral dissertation. Faculty of the Graduate School of the University of Texas at Austin. Austin, Texas, USA.

[29] Anders, S. and Lohaus, L. (2008). Optimized high-performance concrete in grouted connections. Tailor Made Concrete Structures-Walraven & Stoelhorst.